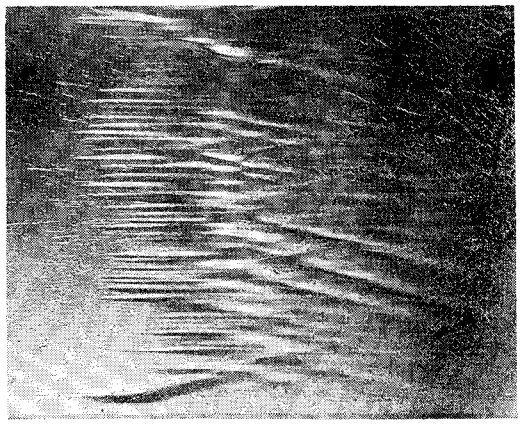

Fig. 2 Spanwise variation of heat transfer for $M = 5.3$ flow over a backward facing step.

boundary-layer thickness over a large range of Mach numbers.[1,2] They were observed in laminar, transitional and turbulent flows. One important practical effect of these vortices is to produce large spanwise variations of the heat transfer and skin friction with local peaks several times larger than the spanwise average value.[3] Examples are shown in Figs. 1 and 2 for a Mach number 5.3 flow over a two-dimensional backward facing step. The striation pattern in Fig. 1, obtained by a sublimation technique of surface flow visualization, demonstrates the spanwise variation of the skin friction. In Fig. 2, grooves scorched into natural wax in the reattachment flow region are indicative of the heat transfer variations. Also seen is the cross-hatched pattern which develops in the turbulent region of the flow. Figure 3 illustrates the skin-friction variations on an axisymmetric hollow cylinder flare model at the same freestream Mach number.

The author has shown that extremely weak initial disturbances existed in the two-dimensional boundary layer upstream of separation because of small imperfections in the leading edge thickness. These were obviously irregularly distributed in the spanwise direction, and the reason why an orderly pattern of pairs of intense counter-rotating vortices develop as the supersonic flow is approaching reattachment is not fully known yet, although an attempt has recently been made[4] to study the stability of a two dimensional stagnation flow at low speeds.

Oil flow visualizations in the reattachment region[1,5] for turbulent supersonic flow over backward facing steps tend to suggest that the flow does not reattach in the classical two-dimensional sense, i.e., on a transverse line along which the skin friction vanishes. It seems rather that flow attachment involves typical three-dimensional singularities (saddle and nodal points of attachment) periodically distributed along a straight line normal to the freestream direction. This is schematically illustrated in Fig. 4 which shows limiting streamlines in the reattachment region as suggested by oil flow visualizations. Nodal and saddles points of attachment are evenly distributed along the "attachment line" AB.

Therefore, although one can conceive that orderly arrays of pairs of counter-rotating vortices of the Görtler type, existing in the free shear layer as a result of streamline curvature, imply this type of flow attachment, one can also conceive that vortices are being developed as a result of this being the only possible type of attachment in the presence of any weak initial disturbance in the approaching boundary layer. It is believed that this approach is worth further investigation.

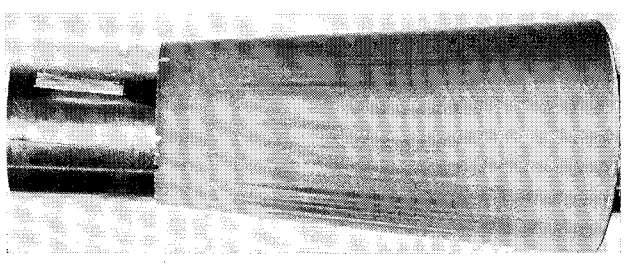

Fig. 3 Spanwise variation of skin friction for $M = 5.3$ flow over a hollow cylinder flare model.

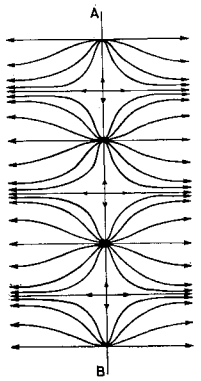

Fig. 4 Schematic configuration of the limiting streamlines in the reattachment region.

References

[1] Ginoux, J., "Experimental Evidence of Three Dimensional Perturbations in the Reattachment of a Two Dimensional Laminar Boundary Layer at M = 2.05," TN 1, 1958, von Kármán Institute, Belgium.

[2] Ginoux, J. "Effect of Mach Number on Streamwise Vortices in Laminar Reattaching Flow; TN 26, 1965, von Kármán Institute, Belgium.

[3] Ginoux, J., "Streamwise Vortices in Laminar Flow," AGARDograph 97, 1965.

[4] Kestin, J. and Wood, R. T., "On the Stability of Two Dimensional Stagnation Flow," *Journal of Fluid Mechanics*, Vol. 44, Pt. 3, 1970.

[5] Roshko, A. and Thomke, G., "Observations of Turbulent reattachment behind an Axisymmetric Downstream-Facing Step in Supersonic Flow," *AIAA Journal*, Vol. 4, No. 6, June 1966, pp. 975–980.

Inequality Constraints in Primer-Optimal, N-Impulse Solutions

D. J. Jezewski* and N. L. Faust†
NASA Manned Spacecraft Center, Houston, Texas

Introduction

THE primer vector approach to the solution of optimal N-impulse trajectory problems has not been extended to solutions in which the imposed constraints are not readily expressed in terms of the control variables. In primer vector solutions,[1–3] the cost is expressed as a sum of the applied impulsive velocity increments. The total differential of this cost is expressed in terms of the differentials of the control variables (that is, the positions and times of all intermediate impulses) and possibly in terms of some variable of the initial and final boundary conditions. Hence, equality constraints at the boundaries of the solution can be readily handled by at most a transformation of coordinates. Inequality constraints at the boundaries of the solution require more attention to the application of the constraints. When the inequality constraint is violated on the boundary, the procedure adopted is to place the control on the boundary and to set the gradient of the cost function with respect to this control to zero. This

Received July 17, 1970; revision received December 30, 1970.

* Aerospace Engineer, Mission Planning and Analysis Division. Member AIAA.

† Aerospace Engineer. Associate Member AIAA.

procedure has been used successfully to solve trajectory problems in which 1) the time is open but bounded and 2) an orbital parameter on the initial and/or final orbit is free but bounded.

Inequality constraints on the orbital elements of the transfer conics (the conics connecting the initial and final boundary conditions) require a different approach in their implementation and solution. One approach is to obtain solutions by means of a penalty function. With this approach, the cost function of the N-impulse solution is appended with a continuous, positive-valued function which is essentially zero for a nonviolation of the constraint and which increases as the constraint is violated. This penalty function must satisfy an additional requirement because the accelerated gradient convergence technique[4,5] used to obtain the optimal N-impulse solutions requires a gradient vector which is a continuous function of the controls. This technique must allow for the oncoming constraint, even though the constraint is not being violated, therefore the measured penalty is still negligible. The formulation of this penalty function and the implementation of this function in the existing optimum multi-impulse rendezvous program comprise the subject matter of this Note.

Penalty Function

The particular double-wall penalty function which is proposed is presented in Fig. 1. A single-wall penalty function would be the left half of the figure. The cost-well penalty function is

$$J_w = J_p + J_q \tag{1}$$

$$J_p = p \exp(1 - \mu^n) \tag{2}$$

$$J_q = q \exp(1 - \delta^m) \tag{3}$$

where $\delta = a/\mu$, $a > 1$, p and q are positive constants, and m and n are positive integers. The penalty function and its derivative purposely do not take on infinite values for $\mu = 1$ because the function or its derivative (or both) is required to be continuous in the interval $0 \leq \mu \leq 1$.

Inequality Constraints in Primer-Optimal Solutions

The cost of an optimal N-impulse solution, when inequality constraints are imposed on the transfer conics, may be written as

$$J = J_o + J_w \tag{4}$$

where

$$J_o = \sum_{i=1}^{N} |\Delta V_i| \tag{5}$$

In Eqs. (4) and (5), J_o is the optimal N-impulse cost function, and J_w is the penalty cost based on the inequality constraints imposed on the transfer conics. For simplicity of nomenclature, a three-impulse problem (N = 3) will be discussed. This approach describes the method of convergence when one interior impulse occurs. The method is extended to multiple-interior-impulse solutions by increasing the dimension of the search procedure.

For an optimal three-impulse solution, the differential cost can be expressed as

$$dJ_o = (\partial J_o/\partial R_m)dR_m + (\partial J_o/\partial t_m)dt_m + (\partial J_o/\partial S_I)dS_I + (\partial J_o/\partial S_F)dS_F \tag{6}$$

where R_m and t_m are the position vector and the time of the intermediate impulse, respectively, and dS_I and dS_F represent possible differential changes in the initial and final state vectors (R,V,t), respectively. The exact form of the gradient vector ∇J_o for the boundary conditions to be considered is not given, but can be obtained from Refs. 1–3.

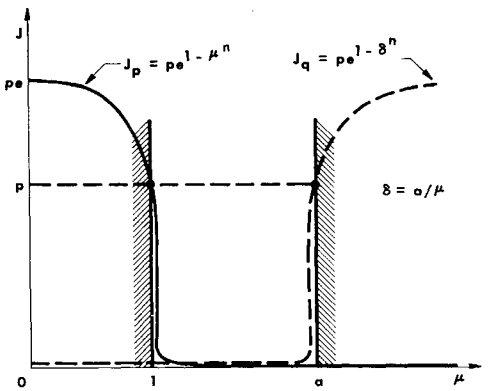

Fig. 1 Double-wall penalty function (cost well).

Because the penalty function J_w is a function of μ only, the differential penalty cost may be written as

$$dJ_w = (\partial J_w/\partial \mu_1)d\mu_1 + (\partial J_w/\partial \mu_2)d\mu_2 \tag{7}$$

where the subscripts 1 and 2 refer to the first and second conics of the three-impulse solution. The parameter μ is a function of only the position and the velocity vectors on the conics. Because the parameter μ can be evaluated at any time on the conics, it is convenient to discuss the problem for a time chosen at the intermediate impulse time. For simplicity of nomenclature, only the penalty function on the first conic will be discussed; thus, the subscripts 1 and 2 will be dropped. The development of the differential penalty cost for the second conic can be derived by a similar technique. If $d\mu$ is expanded in terms of dR_m and dV_m^- (where the superscript minus indicates evaluation at the time immediately before an event t^- and where the superscript plus indicates evaluation at the time immediately after an event t^+), Eq. (7) becomes

$$dJ_w = (\partial J_w/\partial \mu)[(\partial \mu/\partial R_m)dR_m + (\partial \mu/\partial V_m^-)dV_m^-] \tag{8}$$

The term dR_m is the differential of the intermediate position vector [part of the control vector expressed in Eq. (6)] and requires no further transformation. However, the differential dV_m^- must be expressed in terms of the control variables of the optimal N-impulse solution (dR_m, dt_m, dS_I, dS_F). Expansion of dV_m^- results in

$$dV_m^- = \delta V_m^- + \dot{V}_m^- dt_m \tag{9}$$

where $\dot{V}_m^-$ is the acceleration on the first conic at the time t_m^-, and δV_m^- is the perturbation in the velocity vector at

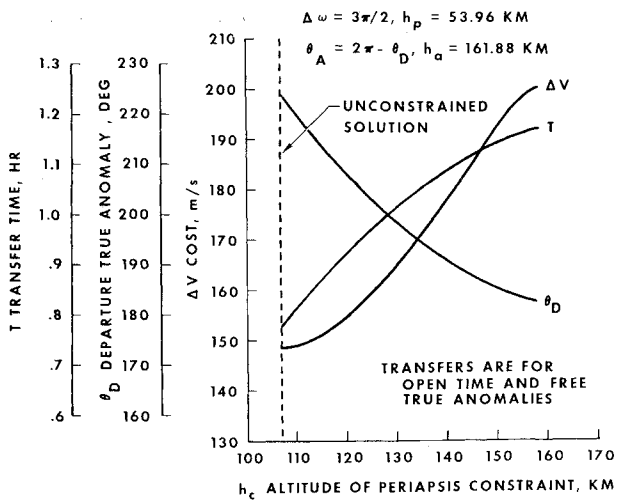

Fig. 2 Constrained transfer between identical coplanar ellipses.

this time as a result of a perturbation in the position vector R_m. Because the acceleration is a function of position ($\dot{V}_m = -R_m/r_m^3$) only and therefore has the same value for both t_m^- and t_m^+, the superscript can be ignored for $\dot{V}_m$. The state-variable perturbations at any two times during the trajectory are related by the state transition matrix. The perturbation in the velocity at the time t_m^- may be written as

$$\delta V_m^- = \phi_{12}^{-1}(t_o,t_m)[\delta R_o^+ - \phi_{11}(t_o,t_m)\delta R_m^-] \quad (10)$$

where the ϕ's represent the 3×3 submatrices of the 6×6 state transition matrix Φ. The perturbations in the position vectors at the times t_o^+ and t_m^- are

$$\delta R_o^+ = dR_o - V_o^+ dt_o \quad \delta R_m^- = dR_m - V_m^- dt_m \quad (11)$$

The use of Eqs. (11) in Eq. (10) eliminates δR_m^- and δR_o^+. Eq. (9) can be used to eliminate δV_m^-. Substituting the result in Eq. (8) eliminates dV_m.

For the first conic of the three-impulse solution, the differential change in the penalty function [Eq. (8)] becomes

$$dJ_w = \frac{\partial J_w}{\partial \mu}\left\{\left(\frac{\partial \mu}{\partial R_m} - \frac{\partial \mu}{\partial V_m^-}\phi_{12}^{-1}\phi_{11}\right)\cdot dR_m + \frac{\partial \mu}{\partial V_m^-}[(\dot{V}_m + \phi_{12}^{-1}\phi_{11}V_m^-)dt_m + \phi_{12}^{-1}(dR_o - V_o^+ dt_o)]\right\} \quad (12)$$

The total differential cost for an optimal three-impulse solution, subject to an inequality constraint on the first arc, is the sum of Eqs. (6) and (12).

Equation (12) is modified for various boundary conditions in the following manner: for a fixed transfer time, set $dt_o = 0$; and for a fixed initial position vector, set $dR_o = 0$. If the initial position vector is no longer considered to be fixed, the variation of the vector δR_o is nonzero.[3] If the time of transfer is fixed, then $dt_o = 0$, and the perturbation in the position vector is due only to a change in the true anomaly in the initial orbit. Thus

$$dR_o = (r_o^2/h_o)V_o^- d\theta_o \quad (13)$$

where r_o and h_o are the magnitudes of the initial radius and angular momentum vectors, respectively, and θ_o is the true anomaly in the initial orbit.

If the initial position vector is considered to be fixed (and transfer time is open), set $dR_o = 0$. The generalized rendezvous problem is characterized by a transfer time which is open, but is functionally dependent upon the motion in the initial and final orbits. The differential of the initial position vector, under these conditions, may be written as $dR_o = V_o^- dt_o$. Once again, similar additional terms occur in the differential dJ_o [Eq. (6)] for each boundary condition which is released.

Example Problem

Consider a constraint on the radius-of-periapsis vector of a transfer conic such that the magnitude of the vector remains above a fixed value r_c. The constraint is considered to be violated whenever the magnitude of the vector is less than or equal to r_c, whether or not the periapsis passage occurs on the transfer conic of the three-impulse solution. The periapsis constraint is written as

$$\mu = [H \cdot H/(1 + |E|)]/r_c \quad (14)$$

where H is the angular momentum vector, and E is the periapsis vector.

The procedure for obtaining an optimal impulsive solution when an inequality constraint is placed on the magnitude of the radius-of-periapsis vector is as follows. In the first phase, the constraint is satisfied, disregarding the optimal impulsive cost J_o and its gradient ∇J_o and using only the penalty function cost J_w and its gradient ∇J_w. Because the penalty function in this phase is formulated as a cost well of width $(a - 1)$ and not as a single-wall function, the constraint parameter μ remains bounded. Once the constraint has been satisfied, the optimal impulsive cost function and its gradient are introduced. Thus, in the second phase, the cost and the gradient are composed of two parts—terms appearing from J_o and J_w. The right-hand side of the cost well, the J_q term, may be dropped in the second phase because the radius of periapsis has an upper boundary at the magnitudes of the initial and the final position vectors. When the function J is minimized away from the boundary, the gradients caused by the constraint are zero, and convergence occurs as if there were no constraint. When the cost function J is minimized at the boundary, the components of the gradients based on the optimal impulsive solution J_o are equal and opposite the direction to the components of J_w. Therefore, the continuity conditions on the primer, on the derivative of the primer, and on the Hamiltonian, across the entire solution, may not be satisfied. Thus, if the primer magnitude is examined on the optimal impulsive solution, a value greater than unity will be found, which indicates that an additional impulse will improve the solution. If an impulse is added and the cycle repeated, a similar result will occur. That is, in the limit, an infinite number of infinitesimal impulses will be required in order to obtain an optimal solution which satisfies the constraint.

Figure 2 presents the results for a periapsis-constrained transfer between two identical coplanar ellipses, with periapsis altitudes of 53.96 km and apoapsis altitudes of 161.88 km. The two ellipses are also misorientated by an angle of 270°. The boundary conditions for these optimal solutions are open transfer time and free departure and arrival true anomalies. The unconstrained optimal, two-impulse solution has a periapsis altitude of 107.1 km with a cost of 148.45 m/sec, a transfer time of 0.78 hr, and a departure true anomaly of 224.3°. As the altitude of the periapsis constraint is increased above this unconstrained value, the cost and transfer time increase, and the departure and arrival true anomalies approach 180°, or the apoapsis positions. The apoapsis point represents a limiting value of the periapsis altitude constraint. Although the maximum value of the primer for the two-impulse extremals increased with an increasing value of the periapsis constraint, the value above unity was insignificant; and when an additional impulse was added, the result was only an infinitesimal decrease in the cost. (Actually, the primer curves for the constrained two-impulse solutions were symmetric, exceeding unity shortly after and before the two impulses.) Hence, for practical purposes, the optimal constrained solutions required only two impulses.

Conclusions

Inequality constraints in primer-optimal, N-impulse solutions can be satisfied by the introduction of a penalty function and its gradient with respect to the appropriate control variables. The constraints may be satisfied between specified boundaries if the penalty function is chosen in the form of a cost well. This general inequality constraint technique may be applied to any conic parameter.

References

[1] Lion, P. M. and Handelsman, M., "Primer Vector on Fixed-Time Impulsive Trajectories," *AIAA Journal*, Vol. 6, No. 1, Jan. 1968, pp. 127–132.

[2] Jezewski, D. J. and Rozendaal, H. L., "Am Efficient Method for Calculating Optimal Free-Space N-Impulse Trajectories," *AIAA Journal*, Vol. 6, No. 11, Nov. 1968, pp. 2160–2165.

[3] Jezewski, D. J., "A Method for Determining Optimal Fixed-Time, N-Impulse Trajectories Between Arbitrary Inclined Orbits," *XIXth International Astronautical Congress Proceedings*,

Vol. 2, *Astrodynamics and Astrionics*, Pergamon Press, PWN—Polish Scientific Publishers, 1970.

[4] Fletcher, R. and Powell, M. J. D., "A Rapidly Convergent Descent Method for Minimization," *The Computer Journal*, Vol. 6, No. 2, July 1963, pp. 163–168.

[5] Johnson, I. L., "Impulsive Orbit Transfer Optimization by an Accelerated Gradient Method," *Journal of Spacecraft and Rockets*, Vol. 6, No. 5, May 1969, pp. 630–632.

An Empirical Model of the Motion of Turbulent Vortex Rings

GARY M. JOHNSON*
Aerospace Research Laboratories, Wright-Patterson Air Force Base, Ohio

DIMENSIONAL arguments indicate that the motion of both axial turbulent puffs (strongly turbulent masses of fluid moving through surroundings with which they readily mix)[1] and turbulent vortex rings[2] will remain similar at all distances from their virtual sources if their spreading rates are linear and their translational velocities decay as the inverse cube of the distance from their respective virtual sources.

This hypothesis appears to be well substantiated for the case of the rapidly spreading turbulent puffs.[1,3] However, the validity of the model is much more difficult to determine for the case of the vortex ring, where the extremely slow ring growth leads to the prediction of very large virtual origins. In fact, recent experiments[4] indicate that measurements would be required at least 1000 diam from the discharging orifice, in order to satisfactorily test the similarity model. Since such measurements have not been made and do not appear to be in the offing, the following empirical model is proposed for use in engineering calculations. Quantitative agreement with experimental results is good to distances on the order of 70 diam from the discharging orifice.

The model is based on measurements of air vortex rings, seeded with a mist of dioctyl phthalate droplets, traveling through quiescent air. The time of flight was recorded by using the signal from a hot-wire anemometer to stop an electronic event timer as the vortex passed the anemometer. The hot-wire circuitry was also used to flash a stroboscope, thereby illuminating the vortex to an open-lensed camera, which recorded its geometry. All measurements were repeated at least thirty times and the mean values were used in further computations.

It was apparent from the data that the behavior of the rings is very accurately described by

$$(t - t_v)/t_0 = C[(x - x_v)/D]^{3/2} \qquad (1)$$

Table 1 Numerical values for the various parameters in Eqs. (1) and (2)

Case	Symbol	D(in.)	Volume of Efflux ($in.^3$)	t_0(sec)	t_v(sec)	x_v(in.)	C	K
1	⊙	4	157.00	.033	.028	-3.781	.131	.943
2	△	4	157.00	.036	-.007	-14.660	.165	.959
3	×	4	78.50	.019	.017	-3.941	.230	.828
4	⊡	4	78.50	.021	.001	15.870	.337	.890
5	▱	4	39.25	.015	.083	7.505	.507	.726

Received December 9, 1970.

* Research Aerodynamicist, Energetics Research Laboratory.

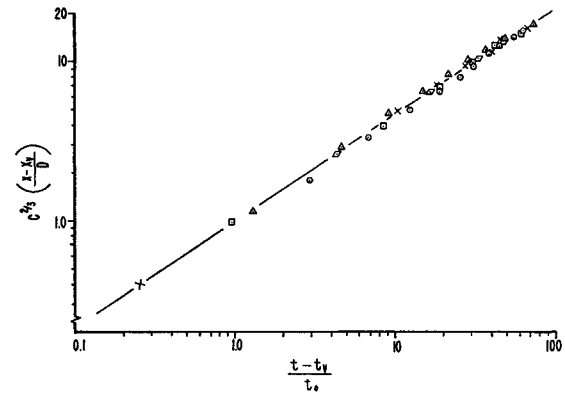

Fig. 1 Comparison of time of flight data with Eq. (1) see Table 1 for an explanation of the symbology.

and

$$2R/D = K[(x - x_v)/D]^{1/6} \qquad (2)$$

where t_v and x_v represent some virtual time and distance respectively, t_0 is the characteristic vortex generation time, R is the vortex ring radius, D is the diameter of the generating orifice, and C and K are constants.

The values of the various parameters for the different initial conditions tested are presented in Table 1. Possible differences between the geometric and kinematic virtual origins of the type discussed by Flora and Goldschmidt[5] have been ignored for the present study. Geometric virtual origins are used throughout.

Quite pleasantly, it may be observed that the values of the virtual time and distance are small. The same data, when fitted to the similarity model, yielded virtual origins for both time and distance which were on the order of the maximum time and distance recorded in the experiments. The small virtual origins obtained when the empirical model is used mean that this model is much less sensitive to small errors in the determination of these virtual origins than is the similarity model.

The data are compared to Eqs. (1) and (2) in Figs. 1 and 2, respectively. As may be observed, the agreement is quite good. The present results have been qualitatively compared to other existing data.[6–8] The agreement is good, except with the data of Krutzsch.[7] However, his results must be viewed skeptically as the measurements were made in an extremely confined chamber.

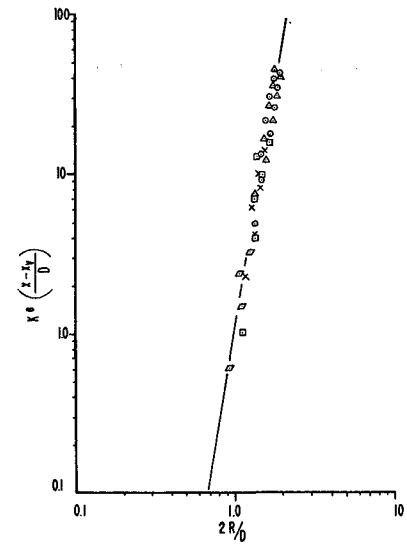

Fig. 2 Comparison of vortex ring radius data with Eq. (2); see Table I for an explanation of the symbology.